Tensile Behaviour of Reinforced UHPFRC Elements under Serviceability Conditions

M. Khorami[1,2], Juan Navarro-Gregori[*, 1], and P. Serna[1]

1: Institute of Science and Concrete Technology, ICITECH, Universitat Politècnica de València, València, 46022, Spain.
2: Universidad UTE, Facultad de Arquitectura y Urbanismo, Calle Rumipamba s/n y Bourgeois, Quito, Ecuador

Corresponding Author: Juan Navarro-Gregori, Associate Prof., Universitat Politècnica de València, Spain.

Email address: juanagre@cst.upv.es Tel: +34-963877007-75617

Orcid: Khorami 0000-0003-4592-0233; Navarro-Gregori 0000-0002-6319-7029; Serna 0000-0001-8754-1165

Abstract

Tension stiffening is an essential effect that influences the behaviour of concrete structures under serviceability conditions, mainly regarding crack control and deflection behaviour. Serviceability conditions can be studied experimentally by running the so-called uniaxial tensile test. This paper reports an extensive experimental research conducted to study the tensile behaviour of reinforced Ultra-High Performance Fibre-Reinforced Concrete (R-UHPFRC) under service conditions by uniaxial tensile testing. The parameters studied were the reinforcement ratio and the steel fibre content in a experimental programme including 36 specimens. Special testing equipment and methodology to measure the post-cracking deformation of R-UHPFRC ties were developed, and special attention was paid to the shrinkage effect. The tensile elements' axial stiffness was approximately parallel to the bare bar response after microcracking formation showing a full tension-stiffening response. The average tensile capacity of the reinforced elements (tension stiffening response) was achieved. Concrete's contribution in the R-UHPFRC ties with the tensile properties deriving from four-point bending tests (4PBTs) on non-reinforced UHPFRC specimens was also compared. The experimental results revealed a slight increase in concrete's contribution with the higher reinforcement ratio. Moreover, the concrete's contribution in the tensile elements was higher than the characteristic tensile properties deriving from 4PBTs.

Keywords: reinforcement, serviceability, tensile elements, tension stiffening, UHPFRC.

Declarations:

- Funding: Project BIA2016-78460-C3-1-R, supported by the Ministry of Economy and Competitiveness of Spain.
- Conflicts of interest / Competing interests: Not applicable
- Availability of data / Material: Not applicable
- Code availability: Not applicable

1. Introduction

For modern constructions and current demands for constructing buildings, some requirements like durability, functionality and aesthetics are important. These requirements are becoming an important key aspect for structural design, and most design codes include mandatory provisions in terms of serviceability conditions. The fundamental requirements associated with serviceability are functionality, user comfort and appearance [1]. However, as these requirements cannot be directly verified, performance criteria like deflection control, vibration control and cracking control are defined to meet these requirements [2]. In other words, serviceability in reinforced concrete structures refers to behaviour upon working loads with particular references made to deflections and cracking. In many structural design situations, and practically in systems such as houses and medium-sized commercial buildings, acceptable structure performance is seldom defined by ultimate limit states, but is controlled by serviceability requirements.

The tensile behaviour of reinforced concrete elements is closely related with the bond property between concrete and the embedded rebars. At a cracked section, the tensile force is mainly carried out by the rebar. However, due to the bond stresses between the rebar and the concrete interface, a fraction of the tensile force is transferred between cracks by the concrete. This effect is termed tension stiffening. In the case of reinforced concrete, the major fraction of the tensile force is carried out by the rebar, and therefore the residual concrete stress at the crack drops to zero rapidly. This effect is termed tension softening and can be characterized by the fracture energy obtained under the tensile stress-crack width relationship. Under serviceability conditions the most important effect that governs the global tensile behaviour is only the tension stiffening effect. On the contrary, UHPFRC provides a significant residual tensile stress in the crack due to the bridging effect of the fibres. Thus, the sum of both tension stiffening and tension softening effects will govern the R-UHPFRC global tensile behaviour. For the sake

of simplicity, the combination of both effects together (tension stiffening and tension softening) is expressed as “tension stiffening” in this paper.

Serviceability verifications are, to some extent, complex to apply because of the cracking phenomenon, tension stiffening, shrinkage, and creep effects. According to the tension stiffening effect, concrete can carry tension between cracks in the reinforced concrete member, which helps to control not only member deformation, but also crack spacing, crack width and the formation of multiple cracks. Consequently, if the reinforced concrete member exhibits major tension stiffening, this effect helps to meet serviceability requirements [3-5].

Crack control in reinforced concrete structures is generally achieved by limiting the increase of the stress in steel reinforcement to an appropriate value that never reaches its yield stress. Many structural concrete design codes specify maximum steel reinforcement stress after cracking and maximum crack width such as [6].

The design serviceability aspects for reinforced UHPFRC structures are not included in CEB-FIP Model Code 2010 (MC2010) [6] and are barely considered in UHPFRC codes or recommendations, such as French code NF P18-470 [7], Japanese standard and guideline JSCE concrete Committee [8], or Swiss standard fprSIA 2052 [9], among others. Thus research in this area is still required as less knowledge is acquired in UHPFRC structures than that acknowledged in RC constructions. By way of example, the French code NF P 18-710 [7] indicates that it is not necessary to perform the control of cracking for strain hardening UHPFRC (T3). However, for the strain softening UHPFRC (T1 and T2) it provides an expression for the calculation of the crack widths in reinforced UHPFRC elements, which includes explicitly both the tension-softening and tension-stiffening effects. On the other hand, the Swiss standard fprSIA 2052 [9] indicates that the verification under serviceability conditions must be carried out by limiting the maximum tensile concrete stresses. For example, in the case of sections under bending forces, the concrete tensile stress is limited to the 90% of the characteristic value of the elastic tensile strength f_t in strain-hardening concretes (UA and UB), while this limitation is reduced to 70% for strain-softening concretes (U0). There is a disparity of criteria when verifying service conditions. Thus, research in this area is still required as less knowledge is acquired in UHPFRC structures than that acknowledged in RC constructions.

In analysis approaches, in which the average stresses and strains used to predict the concrete member behaviour, such as smeared finite elements, truss modelling or a layered beam section analysis, the tension stiffening effect plays a main role and needs to be included in such analyses [10-12]. These types of analysis approaches require a convenient material model for cracked concrete, and the suitable tension stiffening relations for obtaining the stress-strain response of the cracked concrete member. Many constitutive models have been proposed to predict the post-cracking behaviour of conventional reinforcement concrete (RC) [13-17] and fibre-reinforced concrete (FRC) [18-22].

To predict the structural behaviour of UHPFRC concrete members, simple models to represent the tensile behaviour of UHPFRC material are required. Inverse analysis methods can be used to derive the tensile material properties from the load-deflection response obtained from four-point bending tests (4PBTs) [23-26]. In line with this, a new inverse analysis method based on deflection to curvature transformation has been proposed to determine the tensile properties of UHPFRC in the authors' previous research [27, 28]. It remains unclear whether it is possible to also use the tensile properties that directly derive from inverse analysis methods in the analysis of reinforced UHPFRC structures under serviceability conditions.

The present study focuses on the behaviour of reinforced UHPFRC ties under serviceability conditions. The experimental programme consisted of 36 prismatic tensile elements classified into six series with varying reinforcement ratios and two concrete types with different fibre contents. The tension stiffening response and concrete's contribution to the overall response of tensile elements, including the shrinkage effect, were obtained. The influence of the steel fibre content and the reinforcement ratio on tension stiffening under service loads was also studied. Finally, concrete's contribution was compared to the tensile properties deriving from the characterisation tests done using 4PBTs.

2. Experimental programme

The experimental program was developed to carry out the uniaxial tensile test applied to the R-UHPFRC elements [29]. Tensile elements with a square cross-section and one central reinforcement bar along its longitudinal length were prepared. The complete details of specimens are offered in Section 2.2. The experimental programme aimed to characterise the tension stiffening effect of R-UHPFRC elements and to compare it with the tensile properties obtained from bending tests in specimens without reinforcement [27]. The parameters related to fibres, such as type, content and fibre length, affect UHPFRC properties. Therefore, the

influence of each factor on the mix design of concrete should be considered. This study focused on how fibre content influenced tensile behaviour under Serviceability Limit State (SLS) loads. However, the influences of the reinforcement ratio and section dimensions are also presented to provide a comprehensive conclusion. Therefore, the main parameters for this study were section size, reinforcement diameter and fibre content. The test-measured parameters were tensile elongation and tensile force. The test procedure and measurement equipment are explained in Section 2.3. Finally, a study was done to take into account the shrinkage effect.

2.1. Mixture proportion and material properties of UHPFRC

The test programme was conducted with two concrete mixture types that only vary in fibre content terms. The fibre dosage 160 kg/m^3 (concrete C1) and 80 kg/m^3 (concrete C2) were used in this study. The bases of the mixture proportion and aggregate properties were as in previous research conducted by the authors [29, 30]. These chosen dose values were based on both resistant and moderate economic cost criteria. The main components of the mixtures were cement, silica fume, silica flour, fine sand and medium sand. The mix proportion is described in Table 1. The cement used in the experimental programme is Portland cement, obtained from a local plant, and it is classified as CEM I 42.5 R-SRS, with properties according to specification EN 197-1:2011. Its compression strength was 52.5 MPa on the 28th day according to the supplier. The silica sand specific gravity was 2.61 g/cm^3, and two size ranges were used. The fine sand and the medium sand were 0.5 and 0.6-1.2 mm in size. With its small grain size, silica fume and silica flour fill the space in between cement grains, and improve the density and reduce the porosity of UHPFRC [31]. Small steel fibres were herein used with a diameter of 0.2 mm, a length of 13 mm, and a tensile strength beyond 2,000 MPa strength.

A standard horizontal pan mixer was used. Firstly, the dry ingredients, the medium and fine silica sands, silica flour, silica fume and cement were mixed for approximately 1 min. Next water and the superplasticiser were added, and the materials were mixed for 10 min until a homogeneous mixture was obtained and the dry powder mix became a wet paste concrete. The small straight steel fibres were slowly spread by hand into the wet concrete paste in the mixer. The concrete was further mixed for 5 min to ensure proper fibre dispersion. Finally, the fresh UHPFRC material was cast into standard prismatic and cube specimen moulds. As the superplasticizer was used, the concrete did not need to undergo vibration. The specimens from both mixes were cured for 24h at laboratory temperature (25±2ºC) before demoulding. All of the specimens were placed in a high-humidity curing room at 95% relative humidity and temperature of T = 20±2ºC for 28 days.

Six batches were prepared for each concrete type. Four cubic specimens (100 mm), two 150 diameter by 300 mm cylinders and two prismatic specimens (500x100x100 mm) for the compressive strength test, Young modulus test and flexural characterization test were taken from each batch. The average, among all batches, compression strength values of UHPFRC were obtained, which were 154.0 MPa (CV=4.3%) and 139.2 (CV=7.0%) MPa for concrete types C1 and C2, and the average Young's modulus values were 48.4 (CV=1.1%) GPa and 46.5 (CV=1.1%) GPa. Concrete type C1 generally shows a higher modulus of elasticity compared to concrete type C2, but this difference is not significant. Beigi et al.[32], Li [33], and Edgington [34] indicated that using fibres has no significant influence on the Young modulus of concrete, especially with a low fibre content.

The tensile properties of the herein used concrete were obtained by carrying out the 4PBTs and applying an inverse analysis method, which was proposed by the authors in a previous research project [27]. The prismatic specimens were tested under flexural loading. Fig. 1a, and 1b present the test results including the average and characteristic values obtained.

The inverse analysis method was applied to derive constitutive UHPFRC behaviour. The constitutive $\sigma-\varepsilon$ law of UHPFRC can be described with four parameters [27, 28]: cracking strength (f_t), strain at cracking strength ($\varepsilon_{t,el}$), ultimate tensile strength ($f_{t,u}$) and its corresponding strain ($\varepsilon_{t,u}$). In Table2, the average and characteristic tensile properties are presented.

2.2. Specimen preparation

Specimens were made to take a prismatic shape that had a square cross-section with a central rebar. Element length was 1,000 mm, and the rebar was extended 225 mm from both ends. Two complementary rebars were welded to the main rebar (length of 450 mm) to be able to connect the concrete specimen to the steel jaws. In this experimental study, three different cross-section sizes (60, 80, and 100 mm) and two steel reinforcement rebar diameters (Ø10 and Ø12) were used to consider the reinforcement ratio effect on R-UHPFRC behaviour. The nominal yield stress of rebars was 500 MPa. Three specimens were cast for every group of section size and rebar diameter. Thirty-six specimens were tested in the experimental programme. The IDs of the specimens were as follows ϕxx Fxxx Sxx-# , where (Ø) is the rebar diameter in millimetres, (F) is the fibre content in kg/m^3, (S) is the section size in millimetres, and (#) is the number of specimens of each group (see Table 3). Specimen details are shown in Fig. 2a.

2.3. Experimental test setup

A novel test system for performing the uniaxial tensile test has been proposed [30]. The proposed test system and method were suitable for carrying out the experimental test of the R-UHPFRC ties under SLS loads. To apply the tensile force to the concrete specimen, a proposed connection system was used, which included two-piece steel jaws with 2 mm-high indented corrugations assembled by six bolts. The main steel test frame, hydraulic jack, installed specimen and jaw details are shown in Fig. 2b, and 2c. A load cell was placed between the main plate and the end of the anchored rebar to measure force values.

Specimens were tested under manual displacement control at a rate of approximately 0.5 mm/min. Eight displacement transducers (DTs) were installed on the specimen surfaces (four to the right and four to the left of the specimen) to record element elongation during the test, and to capture any bending applied to the specimen due to unforeseen load eccentricities. The length of each DT was 350 mm, and was attached from the centre of specimens to the ends. The position of the installed DTs is shown in Fig. 2d.

3. Experimental results of the R-UHPFRC ties

3.1. Tensile stress-strain behaviour

The experimental method aimed to obtain the average tensile strains and stresses carried by reinforcement and UHPFRC under service loads. The element's total tensile elongation was calculated by the average value recorded by DTs installed on the left and right sides of the specimen (Fig. 2d). It was assumed that the surface deformations of concrete with steel rebar deformation were equal. The test results are presented with the stress-strain curve format insofar as the horizontal axis presents the average tensile strain (ε_{sm}) obtained by the mean elongation recorded by DTs with units mm/m (‰), and the vertical axis shows the total applied force in the tensile element (N) expressed in terms of equivalent concrete tensile stress ($\sigma_{eq,c}$) or equivalent steel stress ($\sigma_{eq,s}$) as follows:

$$\sigma_{eq,c} = \frac{N}{A_c}; \quad A_c = A - A_s$$
$$\sigma_{eq,s} = \frac{N}{A_s} = \rho \cdot \sigma_{eq,c} \tag{1}$$

where (A_s) is the cross-sectional area of reinforcement, (A) is the element's cross-sectional area, and $\rho = A_s/A_c$ is the reinforcement ratio.

3.2. Tensile response

The tensile response of all the specimens with concrete types C1 and C2 is shown in Fig. 3a, and 3b. Each curve represents the average result of three specimens (same section size and rebar diameter). Tensile elongation was measured at the test start time (after the curing and storage times). This means that the results shown in Fig. 3 do not take into account the shrinkage effect occurred so far. The shrinkage effect is discussed in Section 4.3. Diagrams were labelled with reinforcement ratios (ρ) and (ρ / D) to evaluate the influence of the reinforcement ratio and diameter on the tensile elements' general behaviour.

4. Analysis of the results

4.1. Effect of the steel fibre content

The fibre content considerably influenced the tensile properties of UHPFRC. An efficient method to improve the tensile performance of UHPFRC was to increase the amount of fibres in order to increase both tensile strength and toughness. Accordingly, this research aims to investigate the effect of fibre content on the mechanical properties of the two UHPFRC types used: C1 (160 kg/m^3) and C2 (80 kg/m^3).

The increase of the tensile strength was observed by comparing the results obtained for two identical R-UHPFRC ties; e.g., for a given tensile strain (1.5‰), the tensile strength for tensile elements types C1 and C2 with a reinforcement ratio of 1.77% were 12.14 and 9 MPa (see Fig. 3), respectively, where shows enhanced tensile capacity. However, the tensile elements with concrete type C1 showed a higher slope in the elastic region.

Energy absorption is a parameter used to evaluate a material's toughness, which is the material's inherent property that describes the nature of the material to break. Therefore, one way to measure toughness is to calculate the total area under the stress-strain curve with a uniaxial tensile test. In the present study, this concept was applied to define the energy capacity of the tensile elements. Hence in order to evaluate the influence of fibre content on the tensile response of the R-UHPFRC ties, energy absorption (toughness) is calculated as the area under the stress-strain curve, which is herein called energy absorption capacity. Therefore, the area between both curves can be defined as the Increase of Energy Absorption (IEA) due to the fibre content difference.

Figs. 4a to 4f show the tensile stress-strain behaviour of the specimens with identical properties in section size and reinforcement ratio terms for both concrete types. Each curve presents the

average behaviour curve of three identical specimens. The IEA capacity (the area between two curves) shows that the cracked specimens with 160 kg/m^3 present more toughness than those ones with 80 kg/m^3. The average IEA value for all the specimens herein included came close to 21.4%. This increase of the capacity and the improvement in post-cracking behaviour were due to greater fibre bridging over the cracks caused by an additional number of fibres [35, 36]. The obtained result indicated that using a high-fibre dose for the R-UHPFRC ties did not remarkably influence the cracked specimen's energy absorption capacity. So from an economic point of view, employing the double fibre dose in R-UHPFRC (160 and 80 kg/m^3 in this case study) only improved tensile capacity by 21.4% on average. However, the cracking behaviour (crack opening and spacing) of the tensile elements under SLS load and durability performance could lead to a more marked improvement.

4.2. Effect of the reinforcement ratio and rebar diameter

The typical load-strain diagram of a R-UHPFRC tie obtained from the uniaxial tensile test can be described as a bilinear curve with a parabolic part in the interaction zone, as shown in Fig. 5.

The deformation behaviour consists of three stages. The first stage presents the elastic behaviour up until microcracking starts (part OA). The second stage (part AB) refers to microcracking formation. In this stage, cracks are very thin and it is difficult to see them by the naked eye. Additionally, most of the cracks in this stage are internal cracks and cannot reach the specimen surface. In the microcracking stage, element stiffness sharply reduces (refer to the curve slope: β) by increasing deformation. At the end of microcracking (point B), the crack pattern starts to become stable, and a full crack pattern develops (part BC).

The overall tensile response in the crack stabilisation stage (3rd stage) of the RC and FRC ties gradually approaches the bare bar due to the deterioration of the bond surrounding the reinforcement. Given the high bond property of UHPFRC with the reinforcement, the tensile response remains parallel to the bare bar and presents a high tension capacity for the cracked specimen.

One of the most important parameters involved with the cracked specimen's stiffness is the reinforcement ratio and reinforcement diameter. By observing the tension stress-strain relation obtained from the tensile elements (Figs. 3a and 3b), the effect of the aforementioned parameters on tensile deformation behaviour is clearly revealed. The cracked specimen's stiffness (slope of the overall response in the stabilised microcracking stage), which refers to

(γ), was evaluated in this study. To do so, slope (γ) was calculated for all the specimens in the third stage between points B and C. To apply the same criteria to calculate the slope of the curve for all the specimens, two reference points at deformations 0.3‰ and 1.5‰ were chosen (points M and N), where the response curve came close to linear behaviour, as shown in Fig. 6. The main points of the tension response curve obtained from the test results for all the specimens are presented in Table 4.

The start point of microcrack formation (point A) was chosen as the point of the change in the slope of the curve. The elastic tensile stiffness of reinforced UHPFRC (α) was calculated by dividing the (σ_a) by (ε_a). The average proportion of elastic tensile stiffness value for concrete types C1 and C2 (α_{c1}/α_{c2}) calculated for identical specimens was 1.13, which shows that the increased fibre volume ($V_f = 1\%$ to $V_f = 2\%$ in this study) had no significant influence on the elastic tensile stiffness of R-UHPFRC. However, the incorporation of the steel fibres into the concrete matrix improved the bond-slip between the matrix and reinforcement, and increased the elastic stiffness of the UHPFRC ties according to [33, 34, 37].

The stiffness of the cracked R-UHPFRC ties is related to the bridging effect provided by fibres and reinforcement. To evaluate this effect, the variations in (γ) according to the reinforcement ratio (ρ) obtained for the two concrete types are shown in Fig. 7.

The two trend lines obtained for all the specimens for concretes C1 and C2 are nearly parallel. The cracked R-UHPFRC specimens with a higher fibre content show more axial tension stiffness. This increment can be observed as an offset distance between the two trend lines γ_{c1} and γ_{c2} whose value is 31.80 GPa (the increment percentage is 14.80%).

The trend lines for concrete types C1 and C2 (γ_{c1} and γ_{c2}) come very close to the axial stiffness of the bare bar with a value of $E_s = 200\,GPa$. (refer to the red line in Fig. 7). This means that in the third stage, the overall response is almost parallel to the bare bar response. It is worth mentioning that the same experimental tensile response for the R-UHPFRC elements with the parallel curve response by the bare bar response has been observed in the experimental results of other authors [30, 38-42].

4.3. Tension stiffening effect and shrinkage influence

The cracked concrete elements can carry tension between cracks due to the reinforcing bar's bond behaviour. This ability is called the tension stiffening effect, which increases the

element's stiffness before reinforcement yields [19]. Tension stiffening is important for studying the load-deformation characteristic of the reinforced concrete members within the post-cracking range and to calculate crack widths under service loads. In the R-UHPFRC specimens, fibres carry remarkable tensile forces at a crack and effectively increase tension stiffening. Thus the tension stiffening effect is an essential parameter in structural elements designed under SLS conditions because it controls deflections, crack width and crack spacing.

Eurocode 2 [43] indicates that in order to verify the serviceability limit state, the shrinkage effect should be taken into account. Parameters like temperature, curing conditions, mixture properties, material properties and element geometry are involved in the shrinkage strain [44]. However, the high shrinkage strain of UHPFRC needs to be paid special attention for members under tensile stresses. Fig. 8.a and 8b are a qualitative representation of the mean stress-strain curve and tension stiffening response of a R-UHPFRC member, respectively. The shrinkage effects on the tensile response and tension stiffening response are shown. Fig. 8a depicts the stress-strain response in the rebar, while Fig. 8b illustrates the response of concrete.

Creep is a time-dependent characteristic of concrete that causes strains under constant load or stress to increase with time. The effect of creep is usually considered using the concrete effective modulus ($E_{c,eff}$):

$$E_{c,eff} = \frac{E_c(t_0)}{1+\varphi(t,t_0)} \tag{2}$$

where $\varphi(t,t_0)$ is the creep coefficient, which is used to measure the capacity of concrete to creep. The concrete effective modulus can be better evaluated with the modified creep coefficient by applying the relaxation factor [45] or ageing coefficient [46] $\chi(t,t_0)$. The coefficient χ can be estimated at 0.80 for UHPFRC [47]. Hence, the above equation can be written as:

$$E_{c,eff} = \frac{E_c(t_0)}{\left[1+\chi(t,t_0)\varphi(t,t_0)\right]} \tag{3}$$

Several design recommendations and guidelines for UHPFRC suggest values for the creep coefficient. The French code for UHPFRC [47] and Australian design guidelines [48] recommend a creep coefficient of 0.30 for specimens subjected to a standard thermal cure. The creep effect is always present when dealing with shrinkage. Severe creep strains can result in serviceability problems. Hence the equations for calculating the shrinkage effect should include

the creep effect. Nevertheless, the creep effect is not considered within the scope of this paper. This effect should be studied in detail in future research by considering parameters such as cement type, water-cement ratio, concrete strength, relative humidity, temperature effect or size effect among others.

UHPFRC shrinkage would shorten the UHPFRC member without reinforcement, while the embedded reinforcement in the member would restrain shrinkage. It would also lead to a negative "pre-strain" ($\varepsilon_{s,sh}$) with a compressive stress in the steel rebar ($\Delta\sigma_{s,sh}$), and to an initial tensile strain in UHPFRC ($\varepsilon_{c,sh}$) with a tensile stress ($\Delta\sigma_{c,sh}$). Hence the real origin of the mean stress-strain relation would be point O′, as shown in Fig. 8a. The matrix of UHPFRC would be already in tension, even without considering the effects of external actions. Thus the microcracking load level (point A) lowered. The tension stiffening response curve should be modified due to the shrinkage effect by increasing the tension stress caused by shrinkage ($\Delta\sigma_{c,sh}$) and by increasing the concrete tensile strain ($\varepsilon_{c,sh}$).

In this study, we used the equation proposed by Swiss standard fprSIA 2052 code [9, 49] for calculating the free shrinkage (ε_{sh}) magnitude for UHPFRC as follows:

$$\varepsilon_{sh}(t) = \varepsilon_{Us\infty} \cdot e^{\frac{c}{\sqrt{t+d}}} \tag{4}$$

where the values of coefficients are c=-2.48 and d=-0.86, and the age of concrete (t) is expressed as days. The fprSIA 2052 [9] admits that the maximum value for free UHPFRC shrinkage is $\varepsilon_{Us\infty} = 0.6 - 0.8‰$.

Intensive verification tests have been carried out to verify the validity of Eq. 4 at ICITECH facilities. The experimental programme for shrinkage evaluation consisted of three UHPFRC ties with an identical cross-section size (80x80 mm), whereas the steel reinforcement diameter was increased with diameters Ø10 mm, Ø12 mm and Ø16 mm. Accordingly, the longitudinal reinforcement ratio increased by the values of 1.24%, 1.80% and 3.24%. Specimens were cast with UHPFRC with the 160 kg/m^3 fibre content. Three strain gauges were attached to the steel reinforcement to measure the rebar compression strain at the middle and the one-third of each specimen extreme. The average recorded value was used as the compression strain caused by free UHPFRC shrinkage. The measurement process started immediately after casting specimens. Test specimens were cured at room temperature for the first 24 h prior to demoulding. After demoulding, all the specimens were cured at 20±2ºC and 100% relative

humidity for 28 days. It is also worth mentioning that during and after storing specimens in the chamber, the measurement process took place. The average experimental values of the rebar compression strain caused by shrinkage ($\varepsilon_{s,sh}$) after 40 days were 0.341‰, 0.401‰, and 0.411‰ for the specimens with a reinforcement rebar of Ø16 mm, Ø12 mm, and Ø10 mm, respectively. Note that these values are the rebar strain, and it is necessary to apply the uncracked section theory and compatibility conditions to obtain the free shrinkage strain (ε_{sh}).

The free shrinkage strain (ε_{sh}) can be derived as the sum of the steel reinforcement strain and concrete strain:

$$\varepsilon_{sh} = \left|\varepsilon_{s,sh}\right| + \varepsilon_{c,sh} \tag{5}$$

Consequently, the stresses in the steel rebar and concrete caused by free shrinkage are:

$$\Delta\sigma_{s,sh} = \frac{E_s \cdot \varepsilon_{s,sh}}{1 + n \cdot \rho} \tag{6}$$

$$\Delta\sigma_{c,sh} = \frac{n \cdot \rho}{1 + n \cdot \rho} \cdot E_c \cdot \varepsilon_{s,sh} \tag{7}$$

where (n) is the modular ratio (equals E_s / E_c) and (ρ) is the reinforcing steel ratio (equals A_s / A_c). Dividing two sides of Eq. 6 to (E_s) and extract (ε_{sh}) leads to:

$$\varepsilon_{sh} = \varepsilon_{s,sh} \cdot (1 + n \cdot \rho) \tag{8}$$

By employing Eq. 8, the rebar compression strain caused by shrinkage is converted into the free shrinkage strain. Thus the experimental free shrinkage strains are 0.388‰, 0.422‰ and 0.443‰ for specimens with a reinforcement rebar of Ø16 mm, Ø12 mm and Ø10 mm, respectively. The difference between the obtained results allows the conclusion that UHPFRC shrinkage is affected by the reinforcement ratio and cover thickness. E Fehling [38] proposed an expression for ($\varepsilon_{c,sh}$) by considering shrinkage and creep when they develop similarly to each other as follows:

$$\varepsilon_{c,sh} = \frac{\varepsilon_{sh}\left(1 + n.\rho\right)}{1 + n.\rho\left(1 + \chi.\psi\right)} \tag{9}$$

where (χ) is the relaxation factor, which can be estimated with ($\chi = 0.8$), and (ψ) is the creep of UHPFRC.

The free shrinkage strain (ε_{sh}) was also calculated by Eq. 4 at the age of 40 days taking the value 0.8‰ for $\varepsilon_{Us\infty}$. The (ε_{sh}) calculated value was $0.538‰$, which shows a good agreement between the experimental result obtained and the expression proposed by fprSIA 2052 [9]. The following expressions can be used to calculate the tensile stress caused by shrinkage ($\Delta\sigma_{c,sh}$) and the corresponding strain ($\varepsilon_{c,sh}$)

$$\Delta\sigma_{c,sh} = E_c \cdot \varepsilon_{c,sh} \;;\; \varepsilon_{c,sh} = \frac{\varepsilon_{sh} \cdot n \cdot \rho}{1 + n \cdot \rho} \tag{10}$$

The average experimental value of UHPFRC Young's modulus ($E_c = 47\,GPa$), and ($E_s = 200\,GPa$) were used to calculate the initial tensile stress caused by shrinkage for both concrete types. The free shrinkage strain (ε_{sh}) and the corresponding tensile stress and strain caused by shrinkage ($\Delta\sigma_{c,sh}$, $\varepsilon_{c,sh}$) calculated by Eq. 4 are provided in Table 5.

The tension stiffening response was obtained by subtracting the bare bar response from the average load carried by the cracked UHPFRC tensile element. The tension stiffening response was modified with the initial tensile strain in concrete ($\varepsilon_{c,sh}$) and the initial tensile stress ($\Delta\sigma_{c,sh}$) with the values presented in Table 5. The tension stiffening responses for UHPFRC with concrete types C1 and C2, including the shrinkage effect, are presented in Figs. 9a, and 9b. The reinforcement ratio increased from 0.79% to 3.13%. For the reinforcement ratio increment, the average tensile stress in UHPFRC increased from 7.5 to 9.5 MPa for concrete type C1 and from 6.0 to 8.2 MPa for concrete type C2. This increment in the tensile stress in UHPFRC can be related to the higher reinforcement ratio. Therefore, a slight increase of concrete's contribution with the higher reinforcement ratio was observed.

4.4. Comparison between the constitutive model and the tension stiffening response

The tensile stress-strain response of UHPFRC is a fundamental constitutive property of this material, which is one of the most essential aspects of serviceability design and for predicting structural behaviour. Like the R-UHPFRC uniaxial tensile test, it is one of the most appropriate methods for determining the tensile properties of R-UHPFRC. Moreover, this method directly provides the tensile behaviour of reinforced UHPFRC members without having to resort to inverse analysis methodologies. However, the uniaxial tensile test for R-UHPFRC elements is challenging to perform and is very sensitive to several factors, such as boundary conditions, shrinkage effect, loading machine stiffness, specimen imperfection and eccentricity of

reinforcement rebar, stress concentration and end effect [30, 50, 51]. On the contrary, determining the tensile properties of UHPFRC can be easily done by running 4PBTs and using appropriate inverse analysis methods.

The tension stiffening response for all the specimens obtained from the R-UHPFRC ties was compared with the data of the 4PBT simplified inverse analysis results [27] by plotting both together in Figs. 10a, and 10b. The calculated parameters are presented in Table 2.

For the case of the R-UHPFRC specimens with 160 kg/m^3 fibre content (Fig. 10a), a good match appears between the tension stiffening response obtained by the R-UHPFRC uniaxial tensile test and the results of the inverse analysis. Almost all the tension stiffening curves lie between the characteristic and average results of the inverse analysis. The difference between the specimens' tension stiffening responses is due to the different cross-section sizes and rebar diameters, hence the reinforcement ratio effect. As a result, by using the obtained characteristic value, the proposed inverse analysis method exhibits a conservative response.

Based on the obtained experimental results, it was observed that the tensile contribution of the UHPFRC matrix for nearly all the 80 kg/m^3 specimens was located above the average tensile residual strength obtained by inverse analysis from bending tests (Fig. 10b). However, the tensile contribution of the UHPFRC matrix for the 160 kg/m^3 specimens was located between the characteristic and the average values (Fig. 10a). As a result, it can be stated that the fibres' efficiency in the specimens with 80 kg/m^3 is higher than in those with 160 kg/m^3. However, future experimental work should be carried out to confirm the conclusion reached in these tests in a generalised way.

In any case, the UHPFRC concrete's contribution, for any reinforcement ratio and for both considered concrete types, is higher than the characteristic tensile properties derived from the 4PBT simplified inverse analysis.

It can also be seen in Fig. 10 that the scatter is lower for concrete C1. As a consequence of the stochastic nature of concrete cracking, there is often a significant scatter of experimental results. Therefore, the close-up comparison between the tensile properties obtained of 4PBTs and R-UHPFRC tensile elements may include some uncertainties regarding the test configuration, or the time-depending properties of concrete such as shrinkage, creep or stress relaxation. Despite this, the dispersion obtained in the R-UHPFRC tensile elements is in a similar range to that obtained when deriving the tensile properties of 4PBT.

5. Conclusions

The work herein presented provides a study on the behaviour of reinforced UHPFRC ties under serviceability conditions. To this end, the uniaxial tensile test programme, which consists of six series of tensile elements and two concrete types, was carried out. The studied parameters were the reinforcement ratio and fibre content. Tensile behaviour and the tension stiffening response were obtained and modified by considering the shrinkage effect. The tension stiffening response obtained from the tests was compared with the tensile properties obtained from the characterisation of the UHPFRC derived from 4PBT inverse analysis. The derived findings and conclusions are summarised as follows:

1. The overall response of the R-UHPFRC ties showed three well-defined stages for all the tested specimens: (1) elastic behaviour; (2) microcrack formation; (c) microcrack stabilisation. Moreover, no macrocrack formation was observed under the serviceability conditions.
2. The overall experimental response of the R-UHPFRC ties in the microcracking stabilisation stage was almost parallel to the bare bar response, with a nearly full tension stiffening response for both considered concrete types.
3. Increasing the fibre content in UHPFRC (80 kg/m^3 to 160 kg/m^3) improved the energy absorption capacity of the cracked tensile element by approximately 21.4%. Thus for UHPFRC structural applications, designers are recommended to evaluate whether the increase of the tensile response under service loads compensates using a larger fibre content.
4. Concrete's contribution has to be evaluated by taking into account the shrinkage effect. This effect significantly influences the internal stresses that both concrete and reinforcement exhibit, and has to be considered in the serviceability design.
5. A well-defined, but slight, increasing of the concrete's contribution with the increment in the reinforcement ratio was observed.
6. Concrete's contribution in the R-UHPFRC ties is higher than the characteristic tensile value derived from the inverse analysis in the 4PBTs.

Acknowledgements.

This study forms part of Project BIA2016-78460-C3-1-R, supported by the Ministry of Economy and Competitiveness of Spain.

References

1. Burns, C., *Serviceability analysis of reinforced concrete based on the tension chord model.* IBK Bericht, 2012. **342**.
2. Honfi, D., *Design for Serviceability-A probabilistic approach*. 2013: Lund University.
3. Sahamitmongkol, R. and T. Kishi, *Tension stiffening effect and bonding characteristics of chemically prestressed concrete under tension.* Materials and structures, 2011. **44**(2): p. 455-474.
4. Gribniak, V., et al., *Stochastic tension-stiffening approach for the solution of serviceability problems in reinforced concrete: Constitutive modeling.* Computer-Aided Civil and Infrastructure Engineering, 2015. **30**(9): p. 684-702.
5. Muhamad, R., et al., *The tension stiffening mechanism in reinforced concrete prisms.* Advances in Structural Engineering, 2012. **15**(12): p. 2053-2069.
6. Walraven, J.C., *Model Code 2010-Final draft: Volume 1*. Vol. 65. 2012: fib Fédération internationale du béton.
7. AFGC, S., *Bétons fibrés à ultra-hautes performances–Recommandations provisoires.* AFGC, France, 2002.
8. Committee, J.C., *Recommendations for design and construction of high performance fiber reinforced cement composites with multiple fine cracks.* Japan Society of Civil Engineers, Tokyo, Japan, 2008.
9. Cahier Technique, S., *Béton fibré ultra-performant (BFUP)-Matériaux, dimensionnement et exécution.* Projet, 2014.
10. Belarbi, A. and T.T. Hsu, *Constitutive laws of concrete in tension and reinforcing bars stiffened by concrete.* Structural Journal, 1994. **91**(4): p. 465-474.
11. Yankelevsky, D.Z., M. Jabareen, and A.D. Abutbul, *One-dimensional analysis of tension stiffening in reinforced concrete with discrete cracks.* Engineering Structures, 2008. **30**(1): p. 206-217.
12. Stramandinoli, R.S. and H.L. La Rovere, *An efficient tension-stiffening model for nonlinear analysis of reinforced concrete members.* Engineering Structures, 2008. **30**(7): p. 2069-2080.
13. Collins, M.P. and D. Mitchell, *Prestressed concrete structures*. Vol. 9. 1991: Prentice Hall Englewood Cliffs, NJ.
14. Kaklauskas, G., *Integral constitutive model for deformational analysis of flexural reinforced concrete members.* Statyba, 2001. **7**(1): p. 3-9.
15. Hsu, T.T., *Unified theory of reinforced concrete*. 2017: Routledge.
16. Fields, K. and P.H. Bischoff, *Tension stiffening and cracking of high-strength reinforced concrete tension members.* Structural Journal, 2004. **101**(4): p. 447-456.
17. Patel, K., S. Chaudhary, and A. Nagpal, *A tension stiffening model for analysis of RC flexural members under service load.* Computers and Concrete, 2016. **17**(1): p. 29-51.
18. Lee, S.-C., J.-Y. Cho, and F.J. Vecchio, *Tension-Stiffening Model for Steel Fiber-Reinforced Concrete Containing Conventional Reinforcement.* ACI Structural Journal, 2013. **110**(4).
19. Bischoff, P.H., *Tension stiffening and cracking of steel fiber-reinforced concrete.* Journal of materials in civil engineering, 2003. **15**(2): p. 174-182.

20. Amin, A., S.J. Foster, and M. Watts, *Modelling the tension stiffening effect in SFR-RC.* Magazine of Concrete Research, 2016. **68**(7): p. 339-352.
21. Deluce, J.R. and F.J. Vecchio, *Cracking Behavior of Steel Fiber-Reinforced Concrete Members Containing Conventional Reinforcement.* ACI Structural Journal, 2013. **110**(3).
22. Bernardi, P., et al., *Experimental and numerical study on cracking process in RC and R/FRC ties.* Materials and Structures, 2016. **49**(1-2): p. 261-277.
23. Baby, F., et al., *UHPFRC tensile behavior characterization: inverse analysis of four-point bending test results.* Materials and structures, 2013. **46**(8): p. 1337-1354.
24. Lee, S.-C., H.-B. Kim, and C. Joh, *Inverse Analysis of UHPFRC Beams with a Notch to Evaluate Tensile Behavior.* Advances in Materials Science and Engineering, 2017. **2017**.
25. Baby, F., et al. *Identification of UHPFRC tensile behaviour: methodology based on bending tests*. 2013.
26. Baby, F., et al., *Proposed flexural test method and associated inverse analysis for ultra-high-performance fiber-reinforced concrete.* ACI Materials Journal, 2012. **109**(5): p. 545.
27. López, J.Á., et al., *An inverse analysis method based on deflection to curvature transformation to determine the tensile properties of UHPFRC.* Materials and Structures, 2015. **48**(11): p. 3703-3718.
28. López Martínez, J.A., *Characterisation of The Tensile Behaviour of UHPFRC by Means of Four-Point Bending Tests*. 2017.
29. Khorami, M., J. Navarro-Gregori, and P. Serna, *Experimental methodology on the serviceability behaviour of reinforced ultra-high performance fibre reinforced concrete tensile elements.* Strain, 2020. **56**(5): p. e12361.
30. Khorami, M., et al. *A testing method for studying the serviceability behavior of reinforced UHPFRC tensile ties*. in *IOP Conference Series: Materials Science and Engineering*. 2019. IOP Publishing.
31. Lee, N. and D. Chisholm, *Reactive Powder Concrete, Study Report SR 146*. 2005, Ltd. Judgeford, New Zealand.
32. Beigi, M.H., et al., *An experimental survey on combined effects of fibers and nanosilica on the mechanical, rheological, and durability properties of self-compacting concrete.* Materials & Design, 2013. **50**: p. 1019-1029.
33. Li, V.C., *Large volume, high-performance applications of fibers in civil engineering.* Journal of Applied Polymer Science, 2002. **83**(3): p. 660-686.
34. Edgington, J., *Steel fibre reinforced concrete volume B*. 1973, University of Surrey.
35. Löfgren, I., *Fibre-reinforced Concrete for Industrial Construction-a fracture mechanics approach to material testing and structural analysis*. 2005: Chalmers University of Technology.
36. Afroughsabet, V., L. Biolzi, and T. Ozbakkaloglu, *High-performance fiber-reinforced concrete: a review.* Journal of Materials Science, 2016. **51**(14): p. 6517-6551.
37. Buttignol, T.E.T., J. Sousa, and T. Bittencourt, *Ultra High-Performance Fiber-Reinforced Concrete (UHPFRC): a review of material properties and design procedures.* Revista IBRACON de estruturas e materiais, 2017. **10**(4): p. 957-971.
38. Fehling, E., et al., *Ultra-high performance concrete UHPC: Fundamentals, design, examples*. 2014: John Wiley & Sons.
39. Makita, T. and E. Brühwiler, *Tensile fatigue behaviour of Ultra-High Performance Fibre Reinforced Concrete combined with steel rebars (R-UHPFRC).* International Journal of Fatigue, 2014. **59**: p. 145-152.

40. Rauch, M. and V. Sigrist. *Dimensioning of Structures made of UHPFRC*. in *IABSE Symposium Report*. 2010. International Association for Bridge and Structural Engineering.
41. Sigrist, V. and M. Rauch, *Deformation behavior of reinforced UHPFRC elements in tension.* Tailor Made Concrete Structures-Walraven & Stoelhorst (eds), 2008: p. 405-410.
42. Redaelli, D. *Testing of reinforced high performance fibre concrete members in tension*. in *Proceedings of the 6th Int. Ph. D. Symposium in Civil Engineering, Zurich 2006*. 2006. Proceedings of the 6th Int. Ph. D. Symposium in Civil Engineering, Zurich 2006.
43. Institution, B.S., *Eurocode 2: Design of concrete structures: Part 1-1: General rules and rules for buildings*. 2004: British Standards Institution.
44. Gribniak, V., G. Kaklauskas, and D. Bačinskas, *State-of-art review of shrinkage effect on cracking and deformations of concrete bridge elements.* Baltic Journal of Road & Bridge Engineering (Baltic Journal of Road & Bridge Engineering), 2007. **2**(4).
45. Torst, H., *Auswirkungen des superpositionsprinzips auf kriech-und relaxationsprobleme bei beton und spannbeton.* Beton-und stahlbetonbau, 1967. **10**: p. 230-238,261-269.
46. Bazant, Z., *Predictions of concrete effects using age adjusted effective modulus method.* Journal of the American Concrete Institute, 1972. **69**: p. 212-217.
47. AFGC, S., *Bétons fibrés à ultra-hautes performances–Recommandations.* AFGC, France, 2013.
48. Gowripalan, N. and R. Gilbert, *Design guidelines for RPC prestressed concrete beams.* Sydney, Australia: School of Civil and Environmental Engineering, University of New South Wales, 2000.
49. Brühwiler, E. *Swiss Standard SIA 2052 UHPFRC: Materials, Design and Application*. in *4th International Symposium on Ultra-High Performance Concrete and High Performance Materials*. 2016.
50. Ostergaard, L., R. Walter, and J.F. Olesen, *Method for determination of tensile properties of engineered cementitious composites (ECC).* Proceedings of ConMat'05, 2005.
51. Kanakubo, T., *Tensile characteristics evaluation method for ductile fiber-reinforced cementitious composites.* Journal of Advanced Concrete Technology, 2006. **4**(1): p. 3-17.
52. López, J., et al. *Comparison between inverse analysis procedure results and experimental measurements obtained from UHPFRC Four-Point Bending Tests*. in *Proceedings of the 7th RILEM Workshop on High Performance Fiber Reinforced Cement Composites (HPFRCC7)*. 2015.

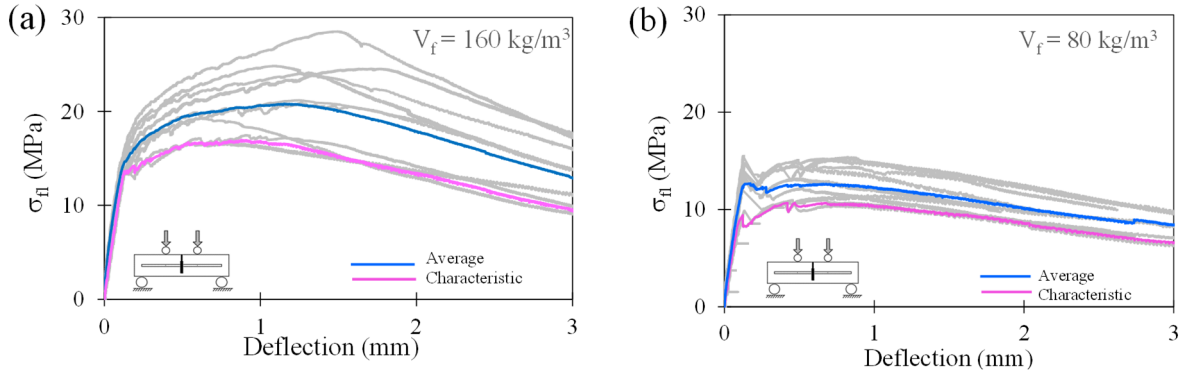

Fig. 1. Equivalent bending stress (σ_{fl}) - midspan deflection for 4PBTs: (a) concrete C1 and (b) concrete C2.

a)

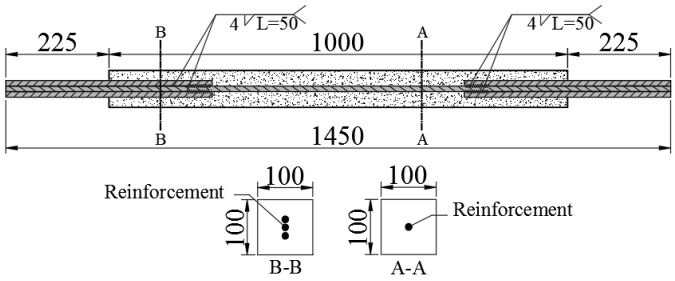

b)

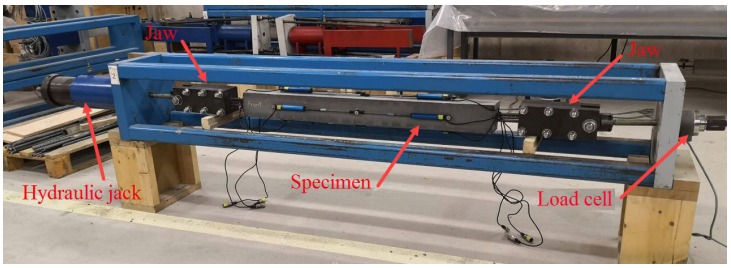

c)

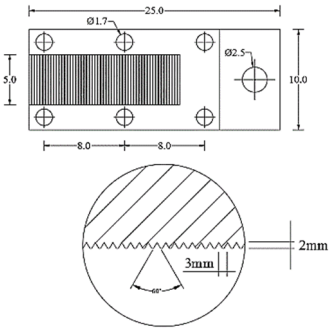

d)

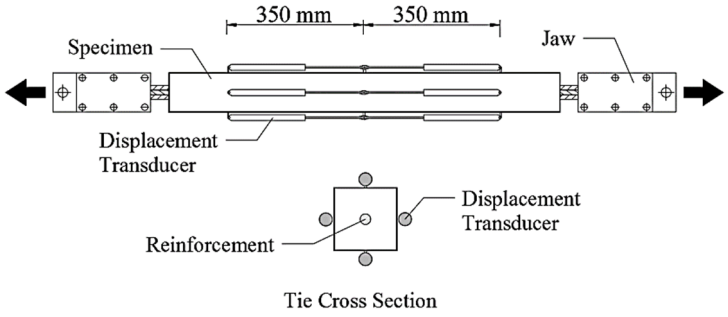

Fig. 2. Uniaxial tensile test equipment: a) Specimen reinforcement details, b) test setup and installed specimen; c) jaw details, d) Position of displacement transducers

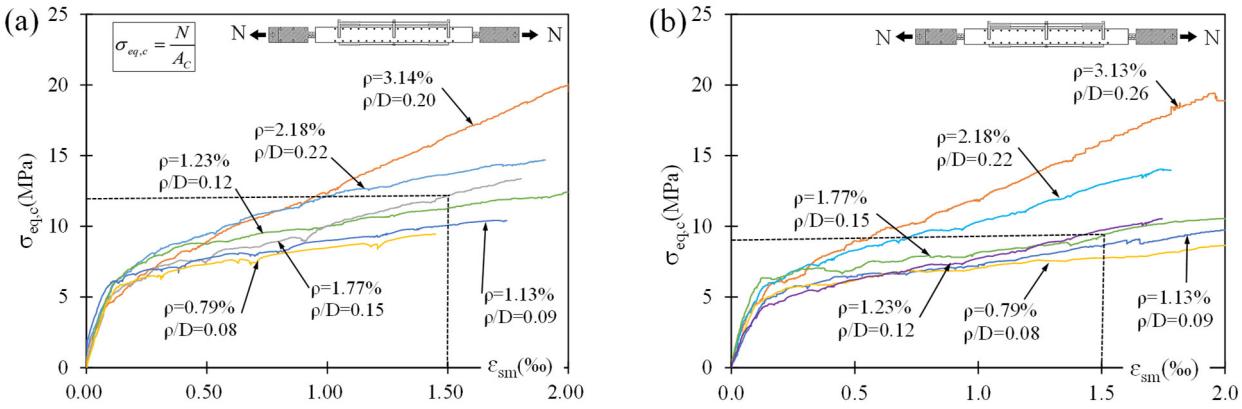

Fig. 3. Tensile response of the R-UHPFRC elements: (a) concrete C1 and (b) concrete C2.

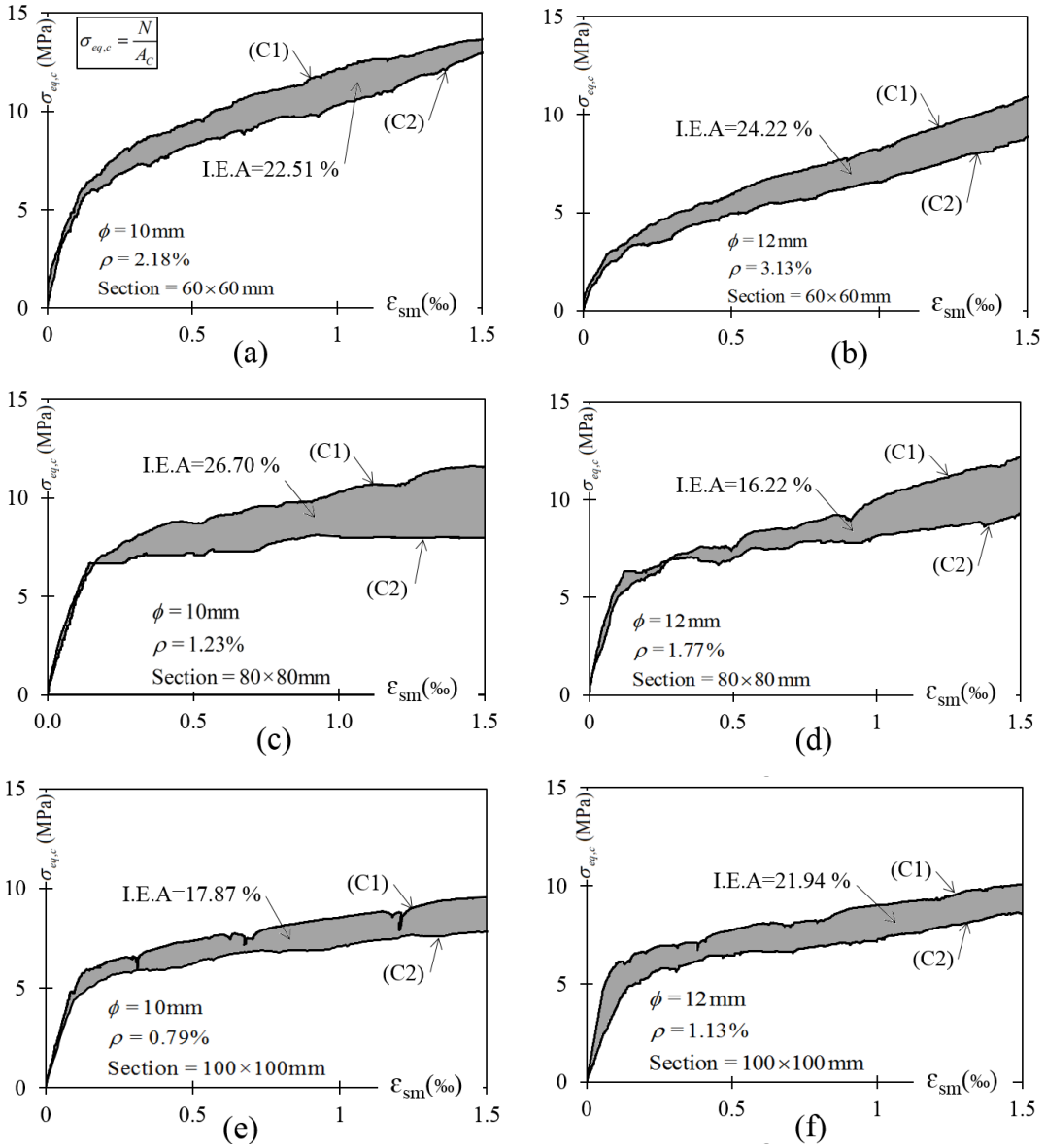

Fig. 4. Increase of Energy Absorption (IEA) due to fibre content increment from 80 to 160 kg/m^3

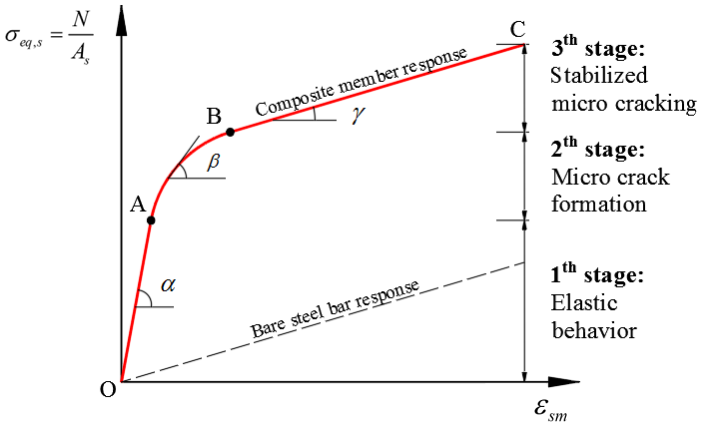

Fig. 5. Load-deformation response of R-UHPFRC tensile element

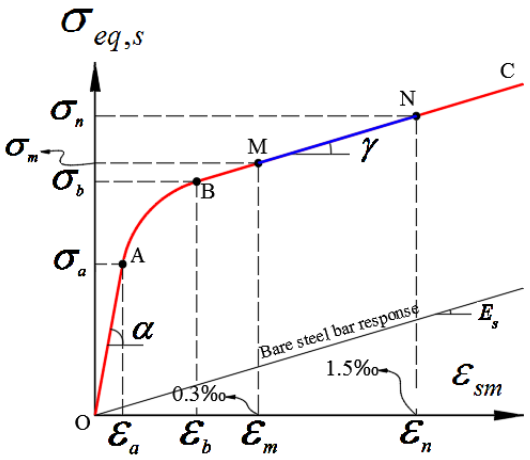

Fig. 6. Slope calculation criteria of the tensile response in the stabilised microcracking stage.

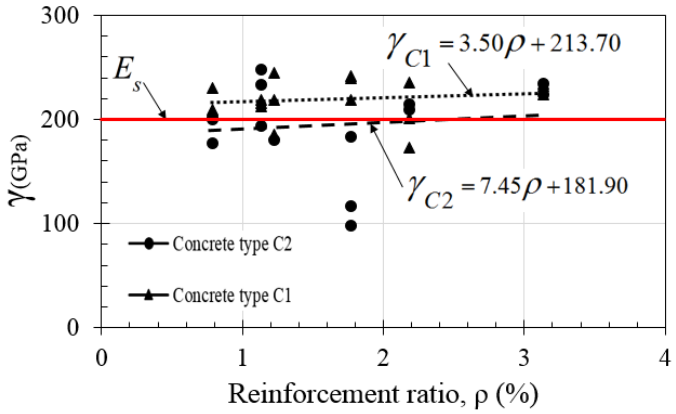

Fig. 7. Influence of the reinforcement ratio (ρ) on the tensile behaviour response

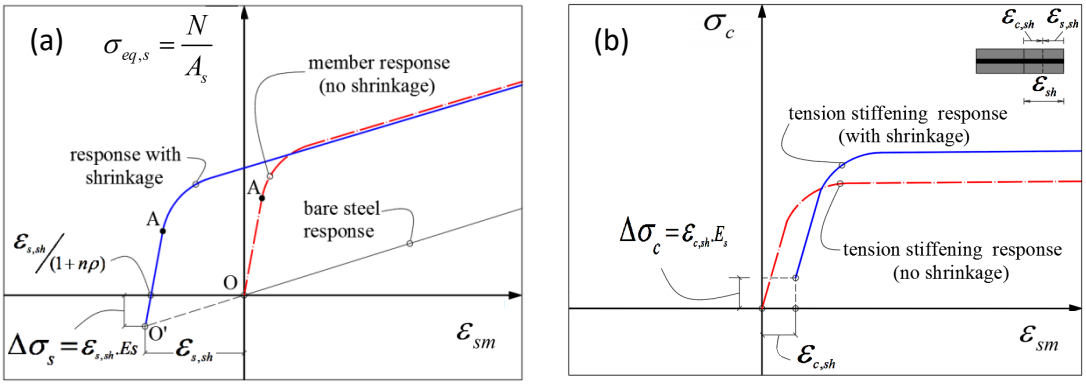

Fig. 8. Shrinkage effect on the response of the R-UHPFRC tie: (a) average stress-strain curve; (b) tension stiffening response

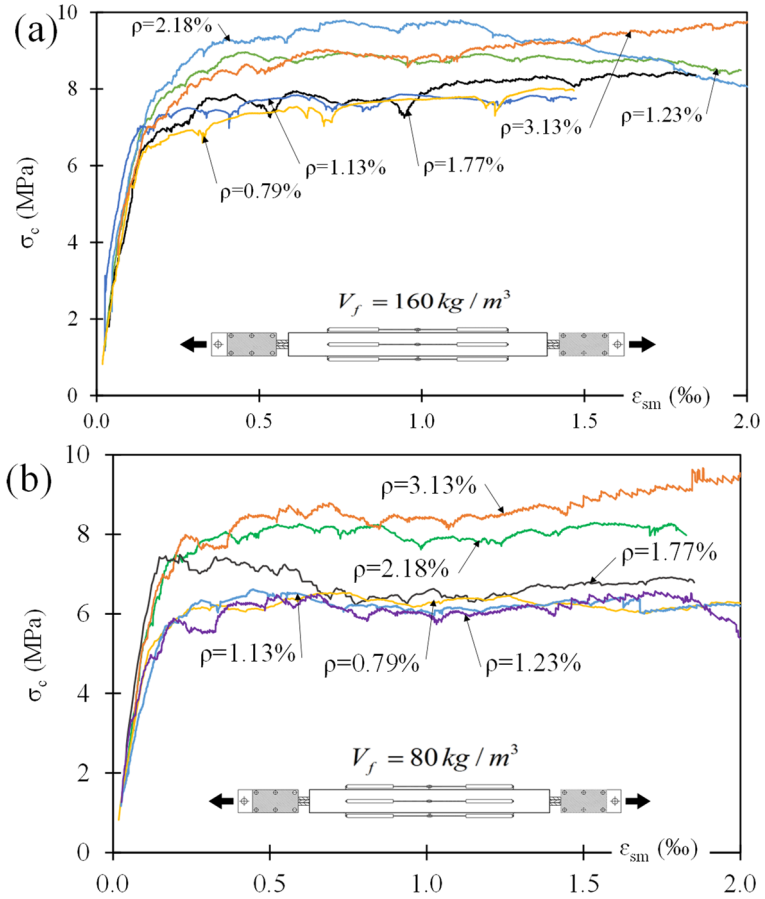

Fig. 9. Concrete's contribution including the shrinkage effect, (a) concrete C1 and (b) concrete C2.

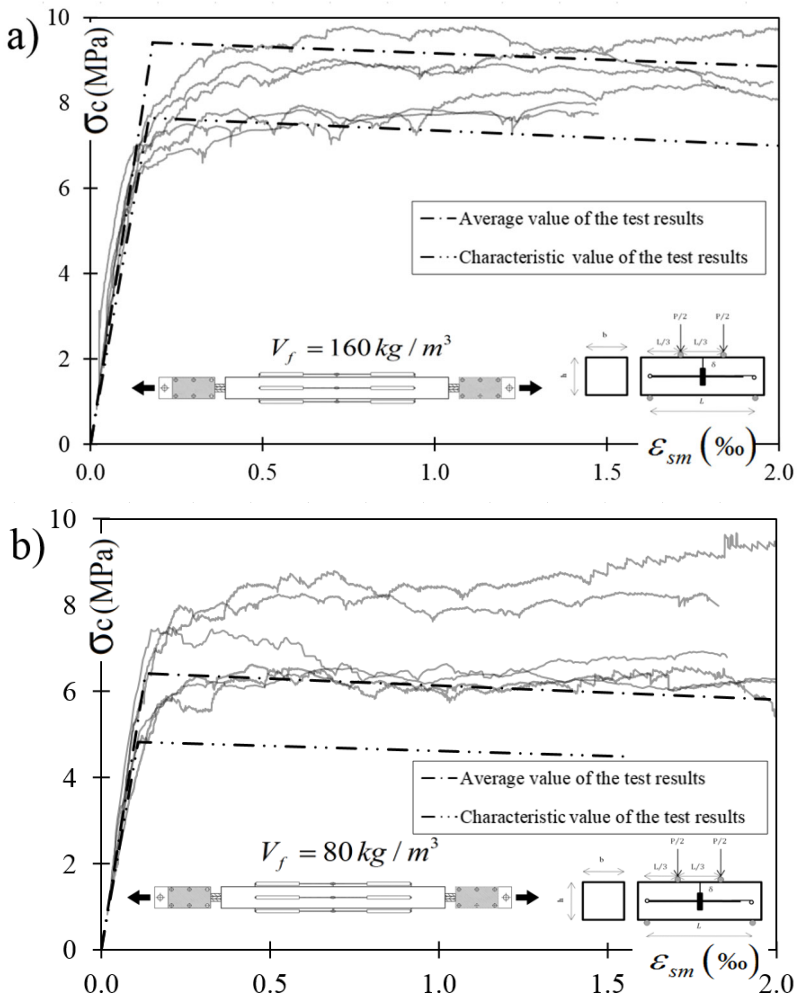

Fig. 10. Comparison between the concrete's contribution and tensile properties from 4PBTs inverse analysis: (a) concrete C1; (b) concrete C2.

Table 1. Mix proportions of UHPFRC for concrete types C1 and C2-unit content (kg/m^3).

Medium sand 0.6–1.2 mm	Fine sand 0.5 mm	Silica flour U-S500	Silica fume (Elkem Microsilica, grade 940)	Cement	Superplasticiser	Water	Fibre content	
565	302	225	175	800	30	160	Concrete type (C1) V_f=2%	160
							Concrete type (C2) V_f=1%	80

Table 2. UHPFRC tensile properties per batch.

Constitutive Relation Model Parameters	f_t (MPa)	$\varepsilon_{t,el}$ (‰)	$f_{t,u}$ (MPa)	$\varepsilon_{t,u}$ (‰)
C1 (V_f=160 kg/m^3)				
Values of characteristic results	7.65	0.17	6.79	4.95
Average result value	9.41	0.18	8.49	6.56
C2 (V_f=80 kg/m^3)				
Values of characteristic results	4.82	0.11	4.48	1.57
Average result value	6.41	0.13	5.81	1.98

Table 3: Description of test specimens.

Concrete type and fibre content				Section Size	Rebar diameter	ρ (%)	Cover (mm)
C1 ($V_f = 160kg/m^3$)		C2 ($V_f = 80kg/m^3$)					
Concrete batch number	Specimen ID	Concrete batch number	Specimen ID				
3	Ø10F160S60-1	3	Ø10F80S60-1	60×60 mm^2	Ø10	2.18	25
2	Ø10F160S60-2	3	Ø10F80S60-2				
5	Ø10F160S60-3	4	Ø10F80S60-3				
6	Ø12F160S60-1	5	Ø12F80S60-1		Ø12	3.13	24
6	Ø12F160S60-2	5	Ø12F80S60-2				
2	Ø12F160S60-3	6	Ø12F80S60-3				
6	Ø10F160S80-1	6	Ø10F80S80-1	80×80 mm^2	Ø10	1.23	35
3	Ø10F160S80-2	6	Ø10F80S80-2				
3	Ø10F160S80-3	5	Ø10F80S80-3				
2	Ø12F160S80-1	4	Ø12F80S80-1		Ø12	1.77	34
5	Ø12F160S80-2	4	Ø12F80S80-2				
3	Ø12F160S80-3	4	Ø12F80S80-3				
1	Ø10F160S100-1	3	Ø10F80S100-1	100×100 mm^2	Ø10	0.79	45
2	Ø10F160S100-2	5	Ø10F80S100-2				
1	Ø10F160S100-3	3	Ø10F80S100-3				
1	Ø12F160S100-1	1	Ø12F80S100-1		Ø12	1.13	44
2	Ø12F160S100-2	1	Ø12F80S100-2				
1	Ø12F160S100-3	2	Ø12F80S100-3				

Table 4. Stress-strain relation curve of the tensile elements for concrete C1 and C2.

Specimen ID	σ_a (MPa)	ε_a (‰)	α (GPa)	σ_b (MPa)	ε_b (‰)	γ (GPa)
Concrete type C1 ($V_f = 160\,\mathrm{kg/m^3}$)						
Ø10F160S60-1	340.97	0.14	2384.41	412.92	0.27	235.23
Ø10F160S60-2	228.27	0.13	1783.36	299.84	0.26	201.22
Ø10F160S60-3	237.44	0.13	1855.00	316.97	0.27	172.89
Ø12F160S60-1	91.38	0.05	1791.76	190.00	0.24	224.34
Ø12F160S60-2	134.92	0.14	992.06	185.41	0.25	232.75
Ø12F160S60-3	155.80	0.09	1832.94	244.69	0.25	234.05
Ø10F160S80-1	520.00	0.11	4727.27	707.00	0.30	245.00
Ø10F160S80-2	512.00	0.15	3413.33	628.00	0.30	185.83
Ø10F160S80-3	483.00	0.15	3220.00	623.00	0.30	218.33
Ø12F160S80-1	279.00	0.09	3100.00	372.00	0.27	241.67
Ø12F160S80-2	339.00	0.15	2306.12	460.00	0.30	240.00
Ø12F160S80-3	222.00	0.07	3171.43	318.00	0.27	219.17
Ø10F160S100-1	603.27	0.09	6703.00	809.81	0.23	230.21
Ø10F160S100-2	643.37	0.10	6433.70	819.18	0.21	209.70
Ø10F160S100-3*	-	-	-	-	-	-
Ø12F160S100-1	458.98	0.10	4413.27	560.92	0.23	215.83
Ø12F160S100-2	448.64	0.08	5340.95	563.35	0.24	218.98
Ø12F160S100-3	536.02	0.13	4254.13	611.95	0.20	212.54
CV (%)	46.96	27.07	49.74	43.04	12.31	8.90
Average	366.71	0.11	3395.46	477.83	0.26	219.87
Concrete type C2 ($V_f = 80\,\mathrm{kg/m^3}$)						
Ø10F80S60-1	232.13	0.11	2210.76	298.03	0.24	214.60
Ø10F80S60-2	244.81	0.12	2003.36	338.73	0.30	209.55
Ø10F80S60-3*	-	-	-	-	-	-
Ø12F80S60-1	143.09	0.11	1266.28	202.45	0.24	224.10
Ø12F80S60-2	144.74	0.13	1130.78	208.65	0.30	234.82
Ø12F80S60-3*	-	-	-	-	-	-
Ø10F80S80-1	281.44	0.08	3518.00	364.56	0.30	78.34
Ø10F80S80-2	350.67	0.12	2922.25	393.51	0.27	59.43
Ø10F80S80-3*	-	-	-	-	-	-
Ø12F80S80-1	267.77	0.07	3771.41	308.27	0.21	183.18
Ø12F80S80-2	285.95	0.10	2749.52	381.41	0.30	116.50
Ø12F80S80-3	363.22	0.12	3078.14	419.50	0.30	98.02
Ø10F80S100-1	574.00	0.09	6377.78	734.22	0.30	202.32
Ø10F80S100-2	551.71	0.11	5254.38	749.80	0.30	177.58
Ø10F80S100-3	601.88	0.12	4853.87	748.93	0.30	200.55
Ø12F80S100-1	364.92	0.11	3475.43	457.04	0.30	194.34
Ø12F80S100-2	459.93	0.11	4181.18	523.20	0.28	233.73
Ø12F80S100-3	267.19	0.10	2754.54	348.00	0.22	247.89
CV (%)	42.65	15.36	43.79	42.08	11.59	40.45
Average	342.23	0.11	3303.18	431.75	0.28	438.82

*These tests failed due to the sliding rebar in the steel jaw.

Table 5. Shrinkage effect on tension stiffening response (Eqs. 1 & 2).

(Concrete age) t	ε_{sh} (‰)	Section size (mm)					
		60x60		80x80		100x100	
		Reinforcement diameter (mm)					
40 days	0.538	Ø 10	Ø 12	Ø 10	Ø12	Ø 10	Ø12
		$\Delta\sigma_{c,sh}$, (MPa)					
		2.19	3.07	1.27	1.80	0.82	1.17
		$\varepsilon_{c,sh}$, (‰)					
		0.047	0.065	0.027	0.038	0.018	0.025
		$\Delta\sigma_{s,sh}$, (MPa)					
		98.31	94.58	102.23	99.98	104.13	102.64
		$\varepsilon_{s,sh}$, (‰)					
		0.492	0.473	0.511	0.500	0.521	0.513